Metrological Characterization of Non-Gaussian Entangled States of Superconducting Qubits

Kai Xu,[1,*] Yu-Ran Zhang,[2,3,*] Zheng-Hang Sun,[1,*] Hekang Li,[1] Pengtao Song,[1] Zhongcheng Xiang,[1] Kaixuan Huang,[1] Hao Li,[1] Yun-Hao Shi,[1] Chi-Tong Chen,[1] Xiaohui Song,[1] Dongning Zheng,[1] Franco Nori,[2,3,4,†] H. Wang,[5,‡] and Heng Fan[1,6,§]

[1]*Institute of Physics, Chinese Academy of Sciences, Beijing 100190, China*
[2]*Theoretical Quantum Physics Laboratory, RIKEN Cluster for Pioneering Research, Wako-shi, Saitama 351-0198, Japan*
[3]*RIKEN Center for Quantum Computing (RQC), Wako-shi, Saitama 351-0198, Japan*
[4]*Physics Department, University of Michigan, Ann Arbor, Michigan 48109-1040, USA*
[5]*Interdisciplinary Center for Quantum Information, State Key Laboratory of Modern Optical Instrumentation, and Zhejiang Province Key Laboratory of Quantum Technology and Device, Department of Physics, Zhejiang University, Hangzhou 310027, China*
[6]*Beijing Academy of Quantum Information Sciences and CAS Center for Excellence in Topological Quantum Computation, University of Chinese Academy of Sciences, Beijing 100190, China*

(Received 29 June 2021; accepted 15 March 2022; published 12 April 2022)

Multipartite entangled states are significant resources for both quantum information processing and quantum metrology. In particular, non-Gaussian entangled states are predicted to achieve a higher sensitivity of precision measurements than Gaussian states. On the basis of metrological sensitivity, the conventional linear Ramsey squeezing parameter (RSP) efficiently characterizes the Gaussian entangled atomic states but fails for much wider classes of highly sensitive non-Gaussian states. These complex non-Gaussian entangled states can be classified by the nonlinear squeezing parameter (NLSP), as a generalization of the RSP with respect to nonlinear observables and identified via the Fisher information. However, the NLSP has never been measured experimentally. Using a 19-qubit programmable superconducting processor, we report the characterization of multiparticle entangled states generated during its nonlinear dynamics. First, selecting ten qubits, we measure the RSP and the NLSP by single-shot readouts of collective spin operators in several different directions. Then, by extracting the Fisher information of the time-evolved state of all 19 qubits, we observe a large metrological gain of $9.89^{+0.28}_{-0.29}$ dB over the standard quantum limit, indicating a high level of multiparticle entanglement for quantum-enhanced phase sensitivity. Benefiting from high-fidelity full controls and addressable single-shot readouts, the superconducting processor with interconnected qubits provides an ideal platform for engineering and benchmarking non-Gaussian entangled states that are useful for quantum-enhanced metrology.

DOI: 10.1103/PhysRevLett.128.150501

Introduction.—The ability to create and manipulate the entangled states of multiparticle quantum systems is crucial for advanced quantum technologies, including quantum metrology [1], quantum error correction [2,3], quantum communications [4,5], quantum simulations [6], and fundamental tests of quantum theory [7]. A universal quantum computer [8] is able to deterministically generate multiparticle entangled states with numerous sequences of single- and 2-qubit operations. However, the conventional step-by-step method is very challenging to scale up and increases exposure to noise. Instead, parallel entangling operations, involving all-to-all connectivity, can efficiently create various types of entangled states and have also been suggested to obtain polynomial or exponential speedups in some quantum algorithms and quantum simulations [9,10]. Realized via the free evolution under a one-axis twisting (OAT) Hamiltonian, the parallel entangling operation first transforms the initial coherent spin state to squeezed spin states [11,12] and then to non-Gaussian entangled states [13], including multicomponent atomic Schrödinger cat Greenberger–Horne–Zeilinger (GHZ) state [14,15]. In the squeezed regime, squeezing of a collective spin, described by Gaussian statistics, represents the improvement of phase sensitivity to SU(2) rotations over the standard quantum limit [1,11,16] and can be characterized by the Ramsey squeezing parameter (RSP) ξ^2_{R} [17]. In the oversqueezed regime, multipartite entanglement of the non-Gaussian spin states can be witnessed by extracting the Fisher information (FI) F [18], related to the phase sensitivity in Ramsey interferometry via the Cramér-Rao bound $(\Delta\theta)^2 \geq 1/F$ [1,11,19]. Furthermore, the non-Gaussian entangled states can be classified by the nonlinear squeezing parameter (NLSP) ξ^2_{NL} [20], extending the concept of spin squeezing to nonlinear observables. Despite many achievements in generating linear spin squeezing (e.g., in Bose-Einstein condensates [21–26], atomic ensembles [27–38], and

trapped ions [39]), the non-Gaussian entangled states, believed to perform higher sensitive quantum phase estimation, quantum simulations [6], and classically intractable quantum algorithms (e.g., Shor's algorithm [40]) are attracting growing interests [41–44].

In this Letter, we measure the NLSP using ten interconnected superconducting qubits, which requires the capability of single-shot readouts of collective spin operators. Compared with the linear RSP and the FI, our experiments help to analyze different classes of complicated non-Gaussian entangled states during the OAT evolution of the multiqubit state. Moreover, by extracting the FI, our experiments achieve a metrological gain, $F/N = 9.89^{+0.28}_{-0.29}$ dB using $N = 19$ qubits, which is larger than those obtained in many other experimental platforms with a much larger number of particles.

Quantum metrology, using quantum resources to yield a higher measurement precision than classical approaches, is one of the most promising applications of quantum technologies [1]. By measuring the RSP, the NLSP, and the FI, we demonstrate quantum enhancement in parameter estimation by using entangled states of superconducting qubits. Compared with the RSP, the experimentally measured NLSP represents greater metrological improvement benefiting from nonlinear observables for both Gaussian and non-Gaussian entangled states. Our work will stimulate interest in non-Gaussian entangled states of quantum many-body systems, which are useful in quantum metrology and quantum information processing.

Experimental device.—In our experiments, 19 addressable transmon qubits (Q_j, with j varied from 1 to 19), capacitively coupled to a resonator bus R, are chosen to effectively engineer a OAT Hamiltonian, see Fig. 1(a) and Refs. [15,45]. By equally detuning selected qubits from the resonator by $\Delta/2\pi \simeq -580$ MHz, the effective system Hamiltonian reads (we set $\hbar = 1$, where $\hbar$ is the Planck's constant h divided by 2π)

$$\hat{H} = \sum_{1\le i<j\le N} \chi_{ij}(\hat{\sigma}_i^+\hat{\sigma}_j^- + \text{H.c.}), \tag{1}$$

where $\hat{\sigma}_j^+$ ($\hat{\sigma}_j^-$) is the raising (lowering) operator of Q_j, and χ_{ij} denotes the qubit-qubit coupling. The all-to-all couplings between the qubits are realized by the superexchange interaction mediated by the bus resonator R [46,47]. As shown in Figs. 1(b) and 1(c) for choosing 10 qubits (Q_j with $j = 1, 2, \ldots, 10$) and all 19 qubits, respectively, the effect of unbalanced qubit-qubit couplings, caused by the few crosstalk couplings between neighboring qubits, can be ignored [15,45]. With N selected qubits initialized at their idle points as $|00\ldots0\rangle_N$, we prepare these qubits in the state $|++\cdots+\rangle_N$ via a $Y_{\pi/2}$ pulse and then detune them equally from the resonator R for the quench dynamics with a time t before the readouts in the same direction [see the experimental pulse sequence in Fig. 1(d)].

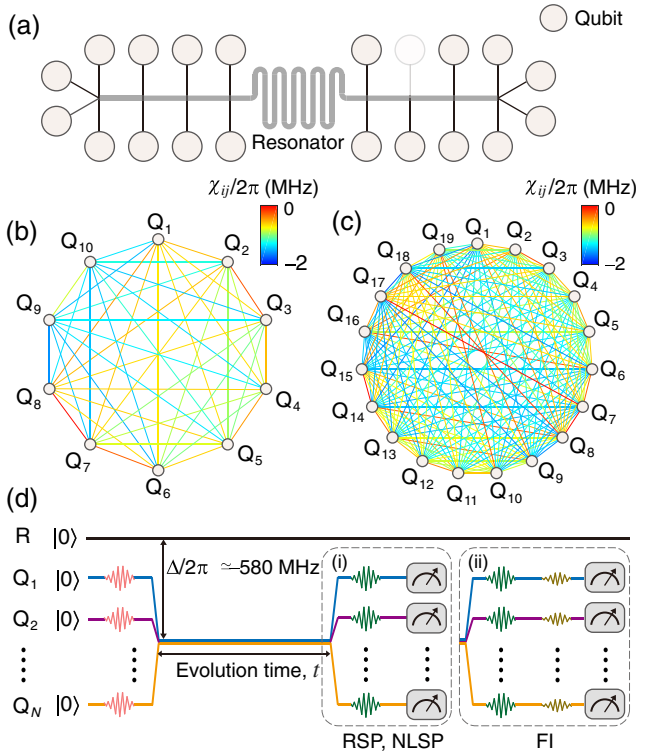

FIG. 1. Superconducting quantum processor and experimental pulse sequence. (a) Simplified schematic of the superconducting quantum processor, showing 19 qubits interconnected by the central bus resonator R. (b),(c) Effective all-to-all coupling strengths χ_{ij} for (b) selected 10 qubits and (c) all 19 qubits. (d) Experimental waveform pulse sequences for detecting (i) the squeezing parameters (RSP and NLSP) and (ii) the FI. Ten or 19 qubits are initially prepared at $|0\rangle$ at their idle points and then transformed to $|+\rangle$ by a collective $Y_{\pi/2}$ gate. After the free evolution with a time t, when all qubits are equally detuned to the resonator R with $\Delta/2\pi \simeq -580$ MHz, all qubits at their idle points are measured in the same direction.

The simultaneous single-shot readouts for all the selected qubits are performed by applying readout pulses to the transmission lines, coupled to the readout resonator of each qubit, yielding the joint probabilities of the outcomes of the collective spin operator in the z direction. Collective spin operators in other directions can be measured by rotating the measurement axes with microwave pulses before readout. Our N-qubit system can be described by a family of linear collective spin operators $\hat{\mathbf{J}} \equiv (\hat{J}_x, \hat{J}_y, \hat{J}_z)$, with $\hat{J}_\beta \equiv \sum_{j=1}^N \hat{\sigma}_j^\beta/2$, and $\hat{\sigma}_j^\beta$ being Pauli matrices for $\beta = x$, y, z. The Hamiltonian in Eq. (1) can be approximately expressed as a OAT one $\hat{H} \simeq -\chi\hat{J}_z^2$.

Measurement of the nonlinear squeezing parameter for ten superconducting qubits.—We need to estimate an unknown parameter θ, imprinted on the time-evolved state ρ_t at time t via unitary evolutions, $\rho_t(\theta) = e^{-i\hat{J}_{\hat{n}}\theta}\rho_t e^{i\hat{J}_{\hat{n}}\theta}$, with $\hat{J}_{\hat{n}} \equiv \hat{n}\cdot\hat{\mathbf{J}}$ being a collective spin operator in the direction $\hat{n} \in \mathbb{R}^3$. For a family of D accessible operators

$\hat{\mathbf{S}} = (\hat{S}_1, \hat{S}_2, \ldots, \hat{S}_D)$, the parameter θ is estimated from the measurement of the observable $\hat{S}_{\hat{m}} = \hat{m} \cdot \hat{\mathbf{S}}$, with $\hat{m} \in \mathbb{R}^D$, as a linear combination of accessible operators. Then, the optimal metrological squeezing parameter of ρ_t for $\hat{\mathbf{S}}$ can be written as [20]

$$\xi^2_{\mathrm{opt}}[\rho_t, \hat{\mathbf{S}}] = \min_{\hat{m}\in\mathbb{R}^D} \min_{\hat{n}\in\mathbb{R}^3} \frac{N(\Delta_{\rho_t}\hat{S}_{\hat{m}})^2}{|\langle[\hat{S}_{\hat{m}}, \hat{J}_{\hat{n}}]\rangle_{\rho_t}|^2}, \tag{2}$$

where $(\Delta_\rho \hat{O})^2 \equiv \langle \hat{O}^2 \rangle_\rho - \langle \hat{O} \rangle^2_\rho$ denotes the variance of the operator $\hat{O}$ with respect to the state ρ. This parameter, $\xi^2_{\mathrm{opt}}[\rho_t, \hat{\mathbf{S}}]$, quantifies the achievable metrological sensitivity enhancement over the standard quantum limit. Its inverse, $\xi^{-2}_{\mathrm{opt}}[\rho_t, \hat{\mathbf{S}}] > \kappa$, with $1 \le \kappa \le (N-1)$, reveals the multiparticle entanglement of at least $(\kappa+1)$ qubits [70]. When the observables are limited to linear collective spin operators $\hat{\mathbf{S}}_{(1)} = \hat{\mathbf{J}}$, the $\xi^2_{\mathrm{opt}}[\rho_t, \hat{\mathbf{J}}]$ reduces to the linear RSP $\xi^2_{\mathsf{R}}[\rho_t]$. We can further define the NLSP $\xi^2_{\mathrm{NL}}[\rho_t]$ with an $\hat{\mathbf{S}}$ that includes not only linear but also nonlinear operators. For example, the second-order NLSP [20] corresponds to the $D = 9$ linear and quadratic collective spin operators in different directions,

$$\hat{\mathbf{S}}_{(2)} = (\hat{J}_x, \hat{J}_y, \hat{J}_z, \hat{J}^2_x, \hat{J}^2_y, \hat{J}^2_z, \hat{J}^2_{xy}, \hat{J}^2_{yz}, \hat{J}^2_{zx}), \tag{3}$$

where $\hat{J}_{\beta\gamma} \equiv (\hat{J}_\beta + \hat{J}_\gamma)/\sqrt{2}$, with $\beta, \gamma \in \{x, y, z\}$.

With the method in Ref. [20] to optimize measurement observables for quantum metrology, we first measure the linear RSP and the NLSP of $N = 10$ qubits during the nonlinear free evolution. The optimal metrological squeezing parameter can be obtained via searching the maximum eigenvalue $\lambda_{\max}$ of a 3×3 matrix $\tilde{\mathcal{M}}[\rho, \hat{\mathbf{S}}]$ as [20]

$$\xi^2_{\mathrm{opt}}[\rho_t, \hat{\mathbf{S}}] = \frac{N}{\lambda_{\max}(\tilde{\mathcal{M}}[\rho_t, \hat{\mathbf{S}}])}, \tag{4}$$

where $\tilde{\mathcal{M}}$ is the submatrix only containing the first three rows and columns of a $D \times D$ matrix $\mathcal{M}$. The matrix $\mathcal{M}$ reads

$$\mathcal{M}[\rho_t, \hat{\mathbf{S}}] = \mathcal{C}^T[\rho_t, \hat{\mathbf{S}}]\mathcal{V}^{-1}[\rho_t, \hat{\mathbf{S}}]\mathcal{C}[\rho_t, \hat{\mathbf{S}}], \tag{5}$$

where $\mathcal{V}[\rho_t, \hat{\mathbf{S}}]$ is the covariance matrix, with elements $\mathcal{V}_{ij}[\rho_t, \hat{\mathbf{S}}] = \langle\{\hat{S}_i, \hat{S}_j\}\rangle_{\rho_t}/2 - \langle\hat{S}_i\rangle_{\rho_t}\langle\hat{S}_j\rangle_{\rho_t}$, and $\mathcal{C}[\rho_t, \hat{\mathbf{S}}]$ is the real-valued skew-symmetric commutator matrix, with elements $\mathcal{C}_{ij}[\rho_t, \hat{\mathbf{S}}] = -i\langle[\hat{S}_i, \hat{S}_j]\rangle_{\rho_t}$. For simplicity, we merely select seven collective spin operators (see Supplemental Material [47]),

$$\hat{\mathbf{S}}_{\mathrm{exp}} = (\hat{J}_x, \hat{J}_y, \hat{J}_z, \hat{J}^2_x, \hat{J}^2_y, \hat{J}^2_{xy}, \hat{J}^2_{zx}), \tag{6}$$

and obtain the time evolution of the NLSP via measuring each element of $\mathcal{V}[\rho_t, \hat{\mathbf{S}}_{\mathrm{exp}}]$ and $\mathcal{C}[\rho_t, \hat{\mathbf{S}}_{\mathrm{exp}}]$ with simultaneous single-shot readouts of ten qubits in different directions (see Supplemental Material [47] for more details). Note that the elements of the matrices $\mathcal{V}$ and $\mathcal{C}$ for the NLSP include the averages of the collective spin operators' third power and fourth power, requiring single-shot readouts of the qubits. The RSP can be simply given by considering the submatrices $\tilde{\mathcal{V}}$ and $\tilde{\mathcal{C}}$, only containing the first three rows and columns of $\mathcal{V}$ and $\mathcal{C}$, respectively. The observable for the optimal metrological squeezing parameter can be obtained as $\hat{S}_{\mathrm{opt}} = \hat{m}_{\mathrm{opt}} \cdot \hat{\mathbf{S}}$, where $\hat{m}_{\mathrm{opt}} = \mathcal{V}^{-1}\mathcal{C}\hat{m}'$, and $\hat{m}' = (n'_1, n'_2, n'_3, 0, \ldots, 0)$, with $\hat{n}_{\max} = (n'_1, n'_2, n'_3)$ being the eigenvector for the maximum eigenvalue of $\tilde{\mathcal{M}}[\rho, \hat{\mathbf{S}}]$ [20,47].

At $t = 34$ and 50 ns, the experimental data of matrices $\mathcal{M}[\rho_t, \hat{\mathbf{J}}]$ and $\mathcal{M}[\rho_t, \hat{\mathbf{S}}_{\mathrm{exp}}]$ for the RSP and the NLSP, respectively, are compared with the numerical predictions in Figs. 2(a) and 2(b). The optimal observable (after normalization) for the RSP at $t = 34$ ns is obtained from experimental data as $0.026\hat{J}_x + 0.463\hat{J}_y - 0.886\hat{J}_z$, and the one for the NLSP at $t = 50$ ns is $-0.025\hat{J}_x + 0.443\hat{J}_y - 0.879\hat{J}_z + 0.070\hat{J}^2_x + 0.002\hat{J}^2_y + 0.020\hat{J}^2_{xy} - 0.157\hat{J}^2_{zx}$. More data for the optimal observables for the RSP and the NLSP during the evolution are shown in the Supplemental Material [47]. The time evolutions of the inverse RSP ξ^{-2}_{R} and the inverse NLSP ξ^{-2}_{NL} are shown in Fig. 2(d), which are compared with the normalized FI F/N. Our results, verifying the hierarchical relationship $\xi^{-2}_{\mathsf{R}} \le \xi^{-2}_{\mathrm{NL}}$, demonstrate that the NLSP, generalizing and improving the RSP with additional quadratic operators, helps to capture a larger set of metrologically useful entangled states. Especially, in the oversqueezed regime (e.g., $t = 82$ ns), the NLSP and the FI identify the multiparticle entangled state with an obvious non-Gaussian distribution in phase space [see the experimental results of the Husimi Q function $Q(\theta, \phi)$ in the rightmost subfigure of Fig. 2(c)], which *cannot* be characterized by the linear RSP. Therefore, the NLSP, measured with single-shot readouts of collective spin operators, is efficient to capture the entanglement of the non-Gaussian state without the need of quantum state tomography.

Extraction of the FI for 10 and all 19 superconducting qubits.—Furthermore, the maximal FI F_{opt}, which quantifies the achievable metrological sensitivity with the optimal linear observable and linear generator, gives an upper bound to the inverse of the optimal metrological squeezing parameter $F_{\mathrm{opt}}/N \ge \xi^{-2}_{\mathrm{opt}}[\rho_t, \hat{\mathbf{S}}]$ [20]. To demonstrate the metrological performance of our superconducting qubits, we experimentally detect the FI by comparing the measurement statistics of the time-evolved states $\tilde{\rho}_t(0)$ and $\tilde{\rho}_t(\theta)$ with and without a small rotation with the generator $\hat{J}_y$ after the optimization rotation along the x axis [Fig. 3(a)]. For a small θ and sufficiently large number of experimental realizations, the FI can be extracted as the coefficient of

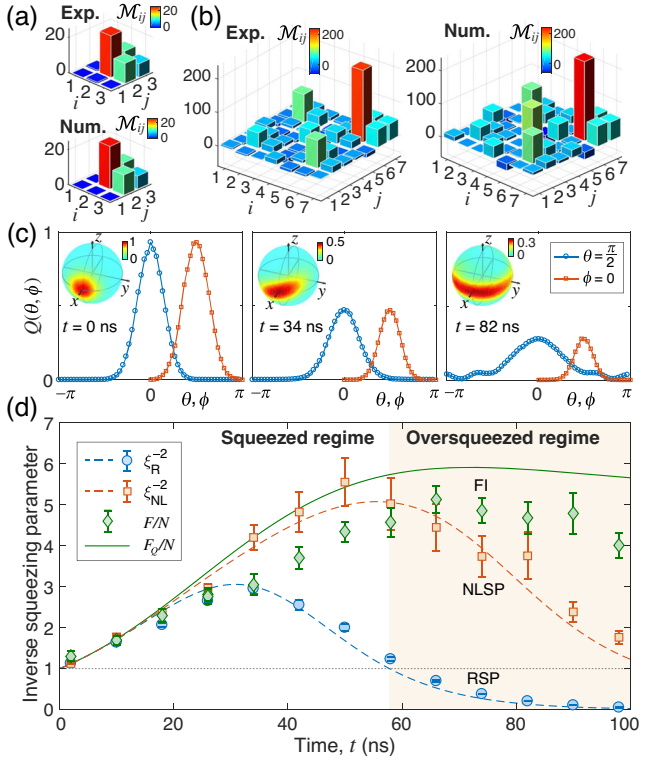

FIG. 2. Linear RSP versus NLSP for ten superconducting qubits. (a),(b) The measured matrices $\mathcal{M}$ to optimize (a) the linear RSP at $t = 34$ ns and (b) the NLSP at $t = 50$ ns, respectively, compared with the numerical simulations. (c) Experimental data of the Husimi Q functions of the states $Q(\theta, \phi)$ against θ and ϕ at specific times with the rotations along the x axis to widen the equatorial distributions. At $t = 0$, 34, and 82 ns, the $Q(\theta, \phi)$ represent the spin-coherent state, the spin-squeezed state, and the non-Gaussian state, respectively. Insets: experimentally measured $Q(\theta, \phi)$ of the evolved states displayed in spherical polar. (d) Time evolutions of the inverse linear RSP ξ_R^{-2}, the inverse NLSP ξ_{NL}^{-2}, with a family of operators $\hat{\mathbf{S}}_{exp}$, and the normalized FI F/N compared with the numerical simulations without decoherence (dashed curves). The experimental procedure for extracting the FI from the squared Hellinger distance is shown in Fig. 3. The green solid curve shows the numerical simulation of the normalized quantum FI, $F_Q/N = 4 \max_{\hat{n} \in \mathbb{R}^3} (\Delta_{\rho_t} \hat{J}_{\hat{n}})^2 / N$, without decoherence, which is the largest normalized FI over all possible measurements and linear generators. The error bars, indicating the standard deviations of the results, are calculated from 200 000 repetitive experimental runs in total (see Supplemental Material [47] for details).

the quadratic term from a polynomial fit to the square of the Hellinger distance [13] [see the experimental results in Fig. 4(a)]:

$$d_H^2(\theta) = \frac{F}{8}\theta^2 + \mathcal{O}(\theta^3), \tag{7}$$

where $d_H^2(\theta) \equiv 1 - \sum_z \sqrt{P_z(0) P_z(\theta)}$, and the sum is the Bhattacharyya coefficient with probability distributions

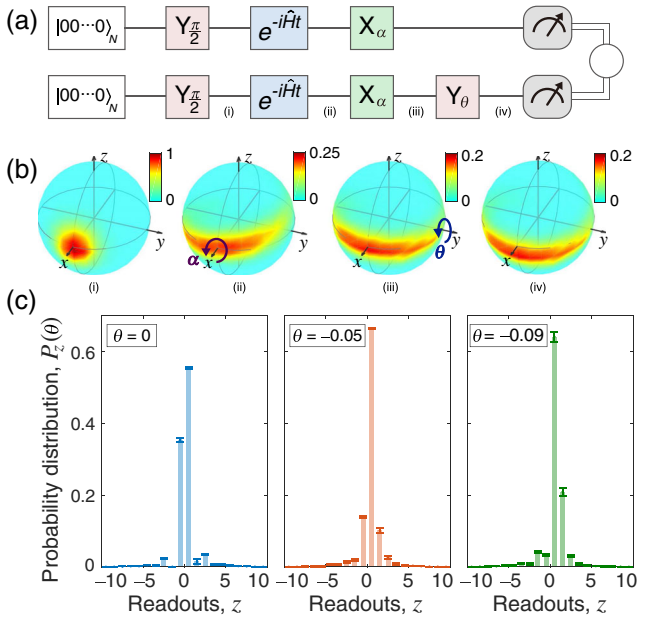

FIG. 3. Experimental procedure for extracting the FI for 19 superconducting qubits. (a) Schematic of the preparation, nonlinear evolution, optimization rotation, measurement, and comparison of the readouts of two states, with and without the collective phase pulse Y_θ, $\exp(-i\hat{J}_y\theta)$, as in the Ramsey interferometer, for the extraction of the FI. (b) Experimental data of the Q functions $Q(\theta, \phi)$ representing the states after (i) the initial preparation, (ii) the nonlinear evolution with $t = 48$ ns, (iii) the collective optimization rotation X_α, $\exp(-i\hat{J}_x\alpha)$, with $\alpha = -0.288$ rad, and (iv) the Ramsey pulse Y_θ, respectively. (c) The probability distributions $P_z(\theta)$ of the measurement observable $\hat{J}_z$ from the single-shot readout of each qubit, for $\theta = 0$, -0.05, and -0.09 rad.

$P_z(0)$ and $P_z(\theta)$ of the observable $\hat{J}_z$ for states $\tilde{\rho}_t(0)$ and $\tilde{\rho}_t(\theta)$, respectively. The experimental results of the probability distributions $P_z(\theta)$ for different values of θ are illustrated in Fig. 3(c). In Fig. 2(d), we show with $N = 10$ qubits that the FI reveals larger multiparticle entanglement, though the RSP and the NLSP increase at long evolution times (e.g., $F/N \geq \xi_{NL}^{-2} \geq \xi_R^{-2}$, with $t \geq 66$ ns). At some times, the measured normalized FI is smaller than the inverse NLSP, because it is difficult in experiments to search for the optimal observable and to apply an infinitesimal phase θ for detecting the quantum FI that gives an upper bound for the inverse NLSP [20]. The maximum normalized FI, $F/N = 5.13 \pm 0.32$ ($7.10^{+0.26}_{-0.28}$ dB), is detected at $t = 66$ ns for $N = 10$ qubits. For $N = 19$ qubits, we measure the FI during the nonlinear time evolution as shown in Fig. 4(c). At $t = 64$ ns, we observe the maximum metrological gain $F/N = 9.75 \pm 0.64$ ($9.89^{+0.28}_{-0.29}$ dB), benefiting from the multiparticle entanglement of non-Gaussian states in the oversqueezed regime.

In addition, the FI is also helpful for obtaining simple integer indicators that capture the extent of multipartite

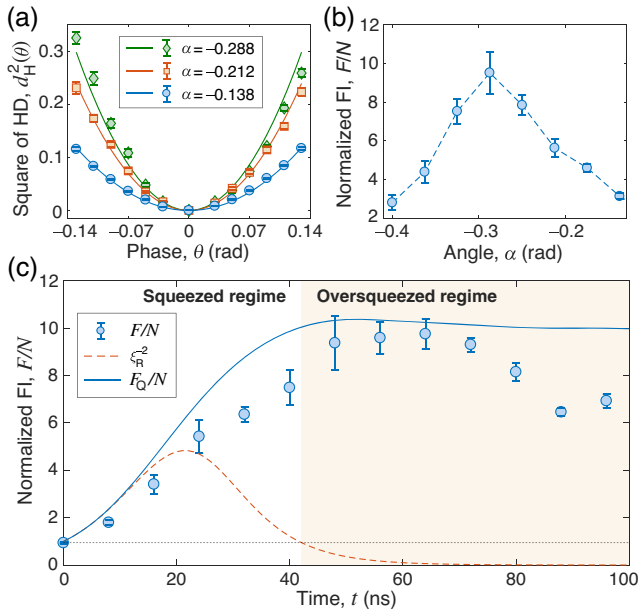

FIG. 4. Quantum-enhanced metrology with 19 superconducting qubits. (a) The squared Hellinger distance (HD) at $t = 48$ ns versus the phase θ in the Ramsey interferometer for different tomography angles $\alpha = -0.288$, -0.212, and -0.138 rad (along the x axis). The solid lines are for the quadratic curve fitting. (b) The normalized FI F/N extracted from the squared Hellinger distance versus α. The optimal angle at $t = 48$ ns is obtained as $\alpha_{\mathrm{opt}} = -0.288$ rad. (c) The time evolution of the normalized FI F/N is compared with the numerical simulations of the inverse RSP (red dashed curve) ξ_R^{-2} and the normalized quantum FI (blue solid curve), $F_Q/N = 4\max_{\hat{n}\in\mathbb{R}^3}(\Delta_{\rho_t}\hat{J}_{\hat{n}})^2/N$, without decoherence. The error bars, indicating the standard deviations of the results, are calculated from about 600 000 repetitive experimental runs in total (see Supplemental Material [47] for details).

correlations: (i) the entanglement depth w describes that at least w parties are entangled; (ii) h inseparability expresses that the system cannot be split into h separable parties [71]. Taking w and h as the width and height of the Young diagram, Dyson's rank $r \equiv w - h$ [72] is a better integer quantifier of multipartite entanglement than either w or h [73], which also indicates the "stretchability" of entanglement [74]. For ten qubits, we obtain from the FI that $r = 3$, saturated by $w = 5$ and $h = 2$. Using 19 qubits, we have $r = 7$, with $w = 11$ and $h = 4$. Our experiment detects positive and relative large Dyson's ranks, implying a large size w of the largest entangled group and a small number h of separable groups.

Numerical details.—Numerical computations are performed using QuTip [75,76] (quantum toolbox in PYTHON) and NumPy. The time evolutions of the system with a Hamiltonian [expressed in Eq. (1)] are numerically simulated using QuTip's master equation solver MESOLVE, where the parameters in Fig. 1(b) and the Supplemental Material [47] are used. Because the evolution time is much shorter than the qubits' energy relaxation time and dephasing time $t \ll T_1, T_2$, we neglect the effect of decoherence in simulations.

Conclusions.—We have demonstrated the characterization of multiparticle entangled states of superconducting qubits utilizing different concepts of entanglement witnesses, including the RSP, NLSP, and FI. With 19 qubits, we have obtained a larger quantum metrological gain over the classical metrology than those obtained in many other platforms with a much larger number of particles. It would imply the potential capability of showing quantum advantages in quantum metrology with interconnected superconducting circuits, as superconducting circuits have been used for the dynamical Casimir effect [77] and to search for dark matter [78]. Owing to the high-fidelity controls and individually addressable single-shot readouts of qubits with long decoherence times, our system is also promising for realizing different quantum algorithms including two-axis twisting spin squeezing [12] and variational quantum simulations [79].

This research was supported by the National Natural Science Foundation of China (Grants No. T2121001, No. 11725419, No. 11934018, No. 11904393, No. 92065114), the Strategic Priority Research Program of Chinese Academy of Sciences (Grant No. XDB28000000), Beijing Natural Science Foundation (Grant No. Z200009), the Nippon Telegraph and Telephone Corporation (NTT) Research, the Army Research Office (ARO) (Grant No. W911NF-18-1-0358), the Japan Science and Technology Agency (JST) [via the Quantum Leap Flagship Program (Q-LEAP), and the Moonshot R&D Grant No. JPMJMS2061], the Japan Society for the Promotion of Science (JSPS) (via the Postdoctoral Fellowship Grant No. P19326, the Grants-in-Aid for Scientific Research (KAKENHI) Grants No. JP19F19326, No JP20H00134), the Asian Office of Aerospace Research and Development (AOARD) (Grant No. FA2386-20-1-4069), and the Foundational Questions Institute Fund (FQXi) (Grant No. FQXi-IAF19-06).

*These authors contributed equally to this work.
†fnori@riken.jp
‡hhwang@zju.edu.cn
§hfan@iphy.ac.cn

[1] V. Giovannetti, S. Lloyd, and L. Maccone, Advances in quantum metrology, Nat. Photonics **5**, 222 (2011).
[2] E. Knill, Quantum computing with realistically noisy devices, Nature (London) **434**, 39 (2005).
[3] E. T. Campbell, B. M. Terhal, and C. Vuillot, Roads towards fault-tolerant universal quantum computation, Nature (London) **549**, 172 (2017).
[4] Z. Zhao, Y.-A. Chen, A.-N. Zhang, T. Yang, H. J. Briegel, and J.-W. Pan, Experimental demonstration of five-photon entanglement and open-destination teleportation, Nature (London) **430**, 54 (2004).

[5] S. Wehner, D. Elkouss, and R. Hanson, Quantum internet: A vision for the road ahead, Science **362**, eaam9288 (2018).
[6] I. M. Georgescu, S. Ashhab, and Franco Nori, Quantum simulation, Rev. Mod. Phys. **86**, 153 (2014).
[7] Z. Wang, H. Li, W. Feng, X. Song, C. Song, W. Liu, Q. Guo, X. Zhang, H. Dong, D. Zheng, H. Wang, and D.-W. Wang, Controllable Switching between Superradiant and Subradiant States in a 10-qubit Superconducting Circuit, Phys. Rev. Lett. **124**, 013601 (2020).
[8] D. Deutsch, Quantum theory, the Church-Turing principle and the universal quantum computer, Proc. R. Soc. A **400**, 97 (1985).
[9] Y. Lu, S. N. Zhang, K. Zhang, W. T. Chen, Y. C. Shen, J. L. Zhang, J.-N. Zhang, and K. Kim, Global entangling gates on arbitrary ion qubits, Nature (London) **572**, 363 (2019).
[10] C. Figgatt, A. Ostrander, N. M. Linke, K. A. Landsman, D. Zhu, D. Maslov, and C. Monroe, Parallel entangling operations on a universal ion-trap quantum computer, Nature (London) **572**, 368 (2019).
[11] J. Ma, X. G. Wang, C. P. Sun, and F. Nori, Quantum spin squeezing, Phys. Rep. **509**, 89 (2011).
[12] M. Kitagawa and M. Ueda, Squeezed spin states, Phys. Rev. A **47**, 5138 (1993).
[13] L. Pezzè, A. Smerzi, M. K. Oberthaler, R. Schmied, and P. Treutlein, Quantum metrology with nonclassical states of atomic ensembles, Rev. Mod. Phys. **90**, 035005 (2018).
[14] C. Song, K. Xu, W. X. Liu, C. P. Yang, S. B. Zheng, H. Deng, Q. W. Xie, K. Q. Huang, Q. J. Guo, L. B. Zhang, P. F. Zhang, D. Xu, D. N. Zheng, X. B. Zhu, H. Wang, Y. A. Chen, C. Y. Lu, S. Y. Han, and J. W. Pan, 10-Qubit Entanglement and Parallel Logic Operations with a Superconducting Circuit, Phys. Rev. Lett. **119**, 180511 (2017).
[15] C. Song, K. Xu, H. K. Li, Y.-R. Zhang, X. Zhang, W. X. Liu, Q. J. Guo, Z. Wang, W. H. Ren, J. Hao, H. Feng, H. Fan, D. N. Zheng, D.-W. Wang, H. Wang, and S.-Y. Zhu, Generation of multicomponent atomic Schrödinger cat states of up to 20 qubits, Science **365**, 574 (2019).
[16] D. J. Wineland, J. J. Bollinger, W. M. Itano, F. L. Moore, and D. J. Heinzen, Spin squeezing and reduced quantum noise in spectroscopy, Phys. Rev. A **46**, R6797 (1992).
[17] D. J. Wineland, J. J. Bollinger, W. M. Itano, and D. J. Heinzen, Squeezed atomic states and projection noise in spectroscopy, Phys. Rev. A **50**, 67 (1994).
[18] S. L. Braunstein and C. M. Caves, Statistical Distance and the Geometry of Quantum States, Phys. Rev. Lett. **72**, 3439 (1994).
[19] H. Cramér, *Mathematical Methods of Statistics* (Princeton University Press, Princeton, NJ, 1946).
[20] M. Gessner, A. Smerzi, and L. Pezzè, Metrological Nonlinear Squeezing Parameter, Phys. Rev. Lett. **122**, 090503 (2019).
[21] C. Orzel, A. K. Tuchman, M. L. Fenselau, M. Yasuda, and M. A. Kasevich, Squeezed states in a Bose-Einstein condensate, Science **291**, 2386 (2001).
[22] J. Estève, C. Gross, A. Weller, S. Giovanazzi, and M. K. Oberthaler, Squeezing and entanglement in a Bose–Einstein condensate, Nature (London) **455**, 1216 (2008).
[23] C. Gross, T. Zibold, E. Nicklas, J. Estève, and M. K. Oberthaler, Nonlinear atom interferometer surpasses classical precision limit, Nature (London) **464**, 1165 (2010).
[24] M. F. Riedel, P. Böhi, Y. Li, T. W. Hänsch, A. Sinatra, and P. Treutlein, Atom-chip-based generation of entanglement for quantum metrology, Nature (London) **464**, 1170 (2010).
[25] X.-Y. Luo, Y.-Q. Zou, L.-N. Wu, Q. Liu, M.-F. Han, M. K. Tey, and L. You, Deterministic entanglement generation from driving through quantum phase transitions, Science **355**, 620 (2017).
[26] Y.-Q. Zou, L.-N. Wu, Q. Liu, X.-Y. Luo, S.-F. Guo, J.-H. Cao, M. K. Tey, and L. You, Beating the classical precision limit with spin-1 Dicke states of more than 10,000 atoms, Proc. Natl. Acad. Sci. U.S.A. **115**, 6381 (2018).
[27] T. Fernholz, H. Krauter, K. Jensen, J. F. Sherson, A. S. Sørensen, and E. S. Polzik, Spin Squeezing of Atomic Ensembles via Nuclear-Electronic Spin Entanglement, Phys. Rev. Lett. **101**, 073601 (2008).
[28] S. Chaudhury, S. Merkel, T. Herr, A. Silberfarb, I. H. Deutsch, and P. S. Jessen, Quantum Control of the Hyperfine Spin of a Cs Atom Ensemble, Phys. Rev. Lett. **99**, 163002 (2007).
[29] J. Appel, P. J. Windpassinger, D. Oblak, U. B. Hoff, N. Kjærgaard, and E. S. Polzik, Mesoscopic atomic entanglement for precision measurements beyond the standard quantum limit, Proc. Natl. Acad. Sci. U. S. A. **106**, 10960 (2009).
[30] T. Takano, Shin-Ichi-Ro Tanaka, R. Namiki, and Y. Takahashi, Manipulation of Nonclassical Atomic Spin States, Phys. Rev. Lett. **104**, 013602 (2010).
[31] I. D. Leroux, M. H. Schleier-Smith, and V. Vuletić, Implementation of Cavity Squeezing of a Collective Atomic Spin, Phys. Rev. Lett. **104**, 073602 (2010).
[32] M. H. Schleier-Smith, I. D. Leroux, and V. Vuletić, States of an Ensemble of Two-Level Atoms with Reduced Quantum Uncertainty, Phys. Rev. Lett. **104**, 073604 (2010).
[33] C. D. Hamley, C. S. Gerving, T. M. Hoang, E. M. Bookjans, and M. S. Chapman, Spin-nematic squeezed vacuum in a quantum gas, Nat. Phys. **8**, 305 (2012).
[34] R. J. Sewell, M. Koschorreck, M. Napolitano, B. Dubost, N. Behbood, and M. W. Mitchell, Magnetic Sensitivity beyond the Projection Noise Limit by Spin Squeezing, Phys. Rev. Lett. **109**, 253605 (2012).
[35] J. G. Bohnet, K. C. Cox, M. A. Norcia, J. M. Weiner, Z. Chen, and J. K. Thompson, Reduced spin measurement back-action for a phase sensitivity ten times beyond the standard quantum limit, Nat. Photonics **8**, 731 (2014).
[36] R. McConnell, H. Zhang, J. Z. Hu, S. Ćuk, and V. Vuletić, Entanglement with negative Wigner function of almost 3,000 atoms heralded by one photon, Nature (London) **519**, 439 (2015).
[37] O. Hosten, N. J. Engelsen, R. Krishnakumar, and M. A. Kasevich, Measurement noise 100 times lower than the quantum-projection limit using entangled atoms, Nature (London) **529**, 505 (2016).
[38] O. Hosten, R. Krishnakumar, N. J. Engelsen, and M. A. Kasevich, Quantum phase magnification, Science **352**, 1552 (2016).
[39] J. G. Bohnet, B. C. Sawyer, J. W. Britton, M. L. Wall, A. M. Rey, M. Foss-Feig, and J. J. Bollinger, Quantum spin

dynamics and entanglement generation with hundreds of trapped ions, Science **352**, 1297 (2016).
[40] P. W. Shor, Polynomial-time algorithms for prime factorization and discrete logarithms on a quantum computer, SIAM J. Comput. **26**, 1484 (1997).
[41] V. Parigi, A. Zavatta, M. Kim, and M. Bellini, Probing quantum commutation rules by addition and subtraction of single photons to/from a light field, Science **317**, 1890 (2007).
[42] F. Haas, J. Volz, R. Gehr, J. Reichel, and J. Estève, Entangled states of more than 40 atoms in an optical fiber cavity, Science **344**, 180 (2014).
[43] H. Strobel, W. Muessel, D. Linnemann, T. Zibold, D. B. Hume, L. Pezzè, A. Smerzi, and M. K. Oberthaler, Fisher information and entanglement of non-Gaussian spin states, Science **345**, 424 (2014).
[44] U. L. Andersen, J. S. Neergaard-Nielsen, P. van Loock, and A. Furusawa, Hybrid discrete- and continuous-variable quantum information, Nat. Phys. **11**, 713 (2015).
[45] K. Xu, Z.-H. Sun, W. X. Liu, Y.-R. Zhang, H. K. Li, H. Dong, W. H. Ren, P. F. Zhang, F. Nori, D. N. Zheng, H. Fan, and H. Wang, Probing dynamical phase transitions with a superconducting quantum simulator, Sci. Adv. **6**, eaba4935 (2020).
[46] S.-B. Zheng, One-Step Synthesis of Multiatom Greenberger-Horne-Zeilinger States, Phys. Rev. Lett. **87**, 230404 (2001).
[47] See Supplemental Material at http://link.aps.org/supplemental/10.1103/PhysRevLett.128.150501 for the comparison of our experimental results with previous works and the details of the experiment, which includes Refs. [48–69].
[48] C. A. Sackett, D. Kielpinski, B. E. King, C. Langer, V. Meyer, C. J. Myatt, M. Rowe, Q. A. Turchette, W. M. Itano, D. J. Wineland, and C. Monroe, Experimental entanglement of four particles, Nature (London) **404**, 256 (2000).
[49] V. Meyer, M. A. Rowe, D. Kielpinski, C. A. Sackett, W. M. Itano, C. Monroe, and D. J. Wineland, Experimental Demonstration of Entanglement-Enhanced Rotation Angle Estimation Using Trapped Ions, Phys. Rev. Lett. **86**, 5870 (2001).
[50] D. Leibfried, B. DeMarco, V. Meyer, D. Lucas, M. Barrett, J. Britton, W. M. Itano, B. Jelenković, C. Langer, T. Rosenband, and D. J. Wineland, Experimental demonstration of a robust, high-fidelity geometric two ion-qubit phase gate, Nature (London) **422**, 412 (2003).
[51] D. Leibfried, M. D. Barrett, T. Schaetz, J. Britton, J. Chiaverini, W. M. Itano, J. D. Jost, C. Langer, and D. J. Wineland, Toward Heisenberg-limited spectroscopy with multiparticle entangled states, Science **304**, 1476 (2004).
[52] D. Leibfried, E. Knill, S. Seidelin, J. Britton, R. B. Blakestad, J. Chiaverini, D. B. Hume, W. M. Itano, J. D. Jost, C. Langer, R. Ozeri, R. Reichle, and D. J. Wineland, Creation of a six-atom "Schrödinger cat" state, Nature (London) **438**, 639 (2005).
[53] I. D. Leroux, M. H. Schleier-Smith, and V. Vuletić, Orientation-Dependent Entanglement Lifetime in a Squeezed Atomic Clock, Phys. Rev. Lett. **104**, 250801 (2010).
[54] A. Louchet-Chauvet, J. Appel, J. J. Renema, D. Oblak, N. Kjaergaard, and E. S. Polzik, Entanglement-assisted atomic clock beyond the projection noise limit, New J. Phys. **12**, 065032 (2010).
[55] Z. L. Chen, J. G. Bohnet, S. R. Sankar, J. Y. Dai, and J. K. Thompson, Conditional Spin Squeezing of a Large Ensemble via the Vacuum Rabi Splitting, Phys. Rev. Lett. **106**, 133601 (2011).
[56] T. Monz, P. Schindler, J. T. Barreiro, M. Chwalla, D. Nigg, W. A. Coish, M. Harlander, W. Hänsel, M. Hennrich, and R. Blatt, 14-Qubit Entanglement: Creation and Coherence, Phys. Rev. Lett. **106**, 130506 (2011).
[57] B. Lücke, M. Scherer, J. Kruse, L. Pezzé, F. Deuretzbacher, P. Hyllus, O. Topic, J. Peise, W. Ertmer, J. Arlt, L. Santos, A. Smerzi, and C. Klempt, Twin matter waves for interferometry beyond the classical limit, Science **334**, 773 (2011).
[58] T. Berrada, S. van Frank, R. Bücker, T. Schumm, J.-F. Schaff, and J. Schmiedmayer, Integrated Mach-Zehnder interferometer for Bose-Einstein condensates, Nat. Commun. **4**, 2077 (2013).
[59] C. F. Ockeloen, R. Schmied, M. F. Riedel, and P. Treutlein, Quantum Metrology with a Scanning Probe Atom Interferometer, Phys. Rev. Lett. **111**, 143001 (2013).
[60] R. J. Sewell, M. Napolitano, N. Behbood, G. Colangelo, F. Martin Ciurana, and M. W. Mitchell, Ultrasensitive Atomic Spin Measurements with a Nonlinear Interferometer, Phys. Rev. X **4**, 021045 (2014).
[61] W. Muessel, H. Strobel, D. Linnemann, D. B. Hume, and M. K. Oberthaler, Scalable Spin Squeezing for Quantum-Enhanced Magnetometry with Bose-Einstein Condensates, Phys. Rev. Lett. **113**, 103004 (2014).
[62] W. Muessel, H. Strobel, D. Linnemann, T. Zibold, B. Juliá-Díaz, and M. K. Oberthaler, Twist-and-turn spin squeezing in Bose-Einstein condensates, Phys. Rev. A **92**, 023603 (2015).
[63] G. Barontini, L. Hohmann, F. Haas, J. Estève, and J. Reichel, Deterministic generation of multiparticle entanglement by quantum Zeno dynamics, Science **349**, 1317 (2015).
[64] K. C. Cox, G. P. Greve, J. M. Weiner, and J. K. Thompson, Deterministic Squeezed States with Collective Measurements and Feedback, Phys. Rev. Lett. **116**, 093602 (2016).
[65] I. Kruse, K. Lange, J. Peise, B. Lücke, L. Pezzè, J. Arlt, W. Ertmer, C. Lisdat, L. Santos, A. Smerzi, and C. Klempt, Improvement of an Atomic Clock Using Squeezed Vacuum, Phys. Rev. Lett. **117**, 143004 (2016).
[66] A. Omran, H. Levine, A. Keesling, G. Semeghini, T. T. Wang, S. Ebadi, H. Bernien, A. S. Zibrov, H. Pichler, S. Choi, J. Cui, M. Rossignolo, P. Rembold, S. Montangero, T. Calarco, M. Endres, M. Greiner, V. Vuletić, and M. D. Lukin, Generation and manipulation of Schrödinger cat states in Rydberg atom arrays, Science **365**, 570 (2019).
[67] R. Krischek, C. Schwemmer, W. Wieczorek, H. Weinfurter, P. Hyllus, L. Pezzé, and A. Smerzi, Useful Multiparticle Entanglement and Sub-Shot-Noise Sensitivity in Experimental Phase Estimation, Phys. Rev. Lett. **107**, 080504 (2011).
[68] L.-Z. Liu, Y.-Z. Zhang, Z.-D. Li, R. Zhang, X.-F. Yin, Y.-Y. Fei, L. Li, N.-L. Liu, F. Xu, Y.-A. Chen, and J.-W. Pan, Distributed quantum phase estimation with entangled photons, Nat. Photonics **15**, 137 (2021).
[69] W. Zhong, Z. Sun, J. Ma, X. Wang, and F. Nori, Fisher information under decoherence in Bloch representation, Phys. Rev. A **87**, 022337 (2013).

[70] L. Pezzè and A. Smerzi, Entanglement, Nonlinear Dynamics, and the Heisenberg Limit, Phys. Rev. Lett. **102**, 100401 (2009).
[71] O. Gühne and G. Tóth, Entanglement detection, Phys. Rep. **474**, 1 (2009).
[72] F. J. Dyson, Some guesses in the theory of partitions, Eureka (Cambridge) **8**, 10 (1944).
[73] Z. Ren, W. Li, A. Smerzi, and M. Gessner, Metrological Detection of Multipartite Entanglement from Young Diagrams, Phys. Rev. Lett. **126**, 080502 (2021).
[74] S. Szalay, *k*-stretchability of entanglement, and the duality of *k*-separability and *k*-producibility, Quantum **3**, 204 (2019).
[75] J. R. Johansson, P. D. Nation, and F. Nori, QuTip: An open-source PYTHON framework for the dynamics of open quantum systems, Comput. Phys. Commun. **183**, 1760 (2012).
[76] J. R. Johansson, P. D. Nation, and F. Nori, QuTip 2: A PYTHON framework for the dynamics of open quantum systems, Comput. Phys. Commun. **184**, 1234 (2013).
[77] C. M. Wilson, G. Johansson, A. Pourkabirian, M. Simoen, J. R. Johansson, T. Duty, F. Nori, and P. Delsing, Observation of the dynamical Casimir effect in a superconducting circuit, Nature (London) **479**, 376 (2011).
[78] K. M. Backes *et al.*, A quantum enhanced search for dark matter axions, Nature (London) **590**, 238 (2021).
[79] C. Kokail, C. Maier, R. van Bijnen, T. Brydges, M. K. Joshi, P. Jurcevic, C. A. Muschik, P. Silvi, R. Blatt, C. F. Roos, and P. Zoller, Self-verifying variational quantum simulation of lattice models, Nature (London) **569**, 355 (2019).